Colloidal glass transition in unentangled polymer nanocomposite melts

2009 J. Phys.: Condens. Matter 21 285102

(http://iopscience.iop.org/0953-8984/21/28/285102)

J. Phys.: Condens. Matter **21** (2009) 285102 (10pp) doi:10.1088/0953-8984/21/28/285102

Colloidal glass transition in unentangled polymer nanocomposite melts

Benjamin J Anderson and Charles F Zukoski

Departments of Chemical and Biomolecular Engineering, University of Illinois, Urbana, IL 61801, USA

E-mail: czukoski@illinois.edu

Received 16 February 2009, in final form 16 May 2009
Published 5 June 2009
Online at stacks.iop.org/JPhysCM/21/285102

Abstract

The linear and non-linear rheology of a high volume fraction particle filled unentangled polymer melt is measured. The particles in the polymer melt behave like hard spheres as the particle volume fraction is raised. At high volume fractions, the suspension develops a plateau elastic modulus. Over the frequency range of the elastic modulus plateau, the viscous modulus develops a minimum and a maximum. The frequencies of the two local extrema initially have critical power law scaling, suggesting the approach of a singular glass transition. At higher volume fractions in excess of the glass transition, the viscous modulus continues to show a well defined minimum and a well defined maximum. The non-linear moduli show a single perturbative yield point beyond which the suspension softens. The yielding behavior of the nanocomposite is shown to be sensitive to the strain frequency and the proximity of the strain frequency to the maximum frequency for the linear viscous modulus from linear rheology which characterizes thermal relaxation of glassy particle clusters in the zero strain limit. The linear and non-linear measurements are compared against a recently developed mechanical theory for colloidal glasses.

(Some figures in this article are in colour only in the electronic version)

1. Introduction

As a supercooled liquid approaches a glassy state, its viscosity changes by many orders of magnitude with small changes in the temperature control parameter [1] (i.e. temperature in molecular fluids and volume fraction in colloidal fluids). The increase in viscosity of colloidal supercooled liquids is due to the localization of particles within a cage of neighbor particles. Understanding the dynamics of particle caging in concentrated colloidal fluids has substantial implications for the design and usage of a wide range of consumer products where particles are used as rheological modifiers and structural enhancers. The liquid to glass transition is unique in that material properties change dramatically as the transition is crossed, but the transition is structurally unidentifiable [2]. As a result, the glass transition is associated with cooperative particle dynamics.

Dynamic scattering experiments carried out as the glass transition is approached show two relaxation processes: a β process due to localized particle diffusion within a cage of nearest neighbor particles and an α process due to particle diffusion out of the cage [3, 4]. The localization of particles by neighbors slows down dynamics and results in enhanced viscosities [5, 6]. Structural relaxation in the supercooled liquid is defined by the characteristic time of cage rearrangements, the α-relaxation time [7]. These relaxation processes depend on the particle volume fraction and diverge in a critical manner as the glass transition is approached [4].

Confocal microscopy studies of hard sphere suspensions near the glass transition confirm the existence of temporal and spatial heterogeneities in supercooled colloidal liquids showing that the glassy dynamics are more complex than initially inferred from scattering experiments [5, 6]. The heterogeneities arise from variation in local particle density that creates clusters of particles with higher particle mobility [5, 6, 8]. The displacement vectors of fast moving particles forming the clusters is correlated showing that the α-relaxation is driven by the cooperative motion of locally fast particle clusters rather than at the single particle level [8]. The size of cooperative rearranging regions increases with volume fraction [6]. Slow clusters have a rigid glass-like structure and form a percolated network [9]. As time progresses,

the percentage of slow clusters having sampled the fast state increases until the percolated network breaks down enabling flow [9]. As the glass transition is approached, the break up time, τ^*, of the percolated network increase [6, 9]. As the glass transition is crossed, the size of cooperative rearranging regions spans the viewing window and fast moving particles appear isolated [6].

The mode coupling theory (MCT) is a heavily studied model which uses equilibrium microstructure information to predict particle localization and the effect of collective processes on dynamics [10–12]. This model has seen extensive testing with hard sphere colloidal fluids and predicts that diffusivities go to zero in a critical manner at the glass transition volume fraction [3, 4]. MCT predicts dynamic arrest above this critical volume fraction. While extensively tested there remains controversy over the idealized nature of the glass transition and the nature of stress relaxation at and above the ideal MCT glass transition. A recent model aimed at attempting to capture relaxation phenomena near and above the glass transition volume fraction has combined the microscopic structural cage correlations of MCT at the single particle level with a non-equilibrium free energy that controls particle dynamics [13, 14]. The theory does not include coupling of dynamic density fluctuations. Therefore, an ideal glass transition plays no role. This model has been further extended to include activated barrier hopping as an ergodicity restoring mechanism with a non-linear stochastic Langevin equation [13–17]. Recently, Kobelev and Schweizer have included the effect of an external stress which acts to remove a free energy minimum and reduce an entropic barrier in the non-equilibrium free energy allowing particles to escape localization [15]. This approach has shown remarkable success in capturing the volume fraction dependence of suspension viscosities up to the ideal glass transition of hard sphere colloidal glasses [13, 14].

Here we present dynamic mechanical measurements on two systems composed of index matched particles suspended in low molecular weight, unentangled, polyethylene oxide (PEO) melts having liquid-like structure factors at all volume fractions studied [18]. The particles in the low MW PEO were recently shown through measurement of the suspension viscosity to interact as effective hard spheres [18]. With increasing volume fraction these suspensions develop classical glassy behavior displaying two characteristic relaxation mechanisms typically associated with a β relaxation process of particles diffusing within a cage of nearest neighbors and an α relaxation process associated with release from cages. Critical behavior with power law divergence is observed in the frequencies characterizing these relaxations extrapolating to an idealized glass transition at an effective hard sphere volume fraction of 0.583. The suspensions also show continued relaxation behavior above this volume fraction indicating the presence of relaxation mechanisms at work above the critical volume fraction. We compare our rheological characterization of the nanocomposite suspensions to the elastic modulus and yield stress predicted for hard spheres by Kobelev and Schweizer. To our knowledge, this is the first mechanical characterization of the linear and non-linear glassy dynamics in a particle suspension capturing both the α and β relaxations. Previous studies of the mechanical properties of glassy particle suspensions have not been able to access experimentally the dynamics due to the long time scales of the relaxation process. In the present system, the rheological properties of the dispersing polymer and the small size of the particles allow the relaxation dynamics to be seen within the viewable frequency window.

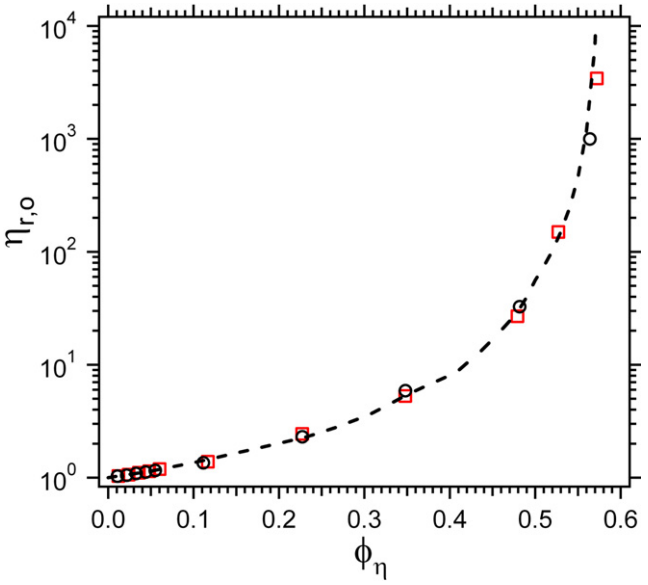

Figure 1. The low shear viscosity plotted versus ϕ_η for PEO400 (○) and PEO1000 (□). The dashed line is a smooth curve through data for experimental hard spheres [26].

2. Experimental methods

Suspensions are made by dispersing 44 ± 4 nm Stöber silica in low molecular weight PEO melts using solution intercalation mixing. The polydispersity of the particles frustrates crystallization seen in more monodisperse particle suspensions for $0.50 \leqslant \phi \leqslant 0.55$. Ethyl alcohol is the added solvent for mixing and is evaporated in a vacuum oven. The unentangled PEO–silica nanocomposites have low shear viscosities that compare well to other model hard sphere suspensions (figure 1). PEO with a molecular weight of 400 and 1000 are Newtonian fluids within the studied range of shear rate and frequency with viscosities of 16 cP and 35 cP, respectively. In the melt, the silica particles have a larger effective size due to the adsorption of PEO to the particle surface such that it forms an immobilized layer that increases the particle hydrodynamic size. The thickness of the immobilized layer scales with polymer radius of gyration, R_g, such that the low shear viscosity of two molecular weights of PEO nanocomposites collapsed onto a single curve that agrees with experimental hard sphere suspension viscosity at all particle concentrations. The collapse of the nanocomposite viscosities onto the hard sphere curve is accomplished by adjusting the core silica volume fraction, ϕ_c, to account for the adsorbed layer allowing us to define an effective

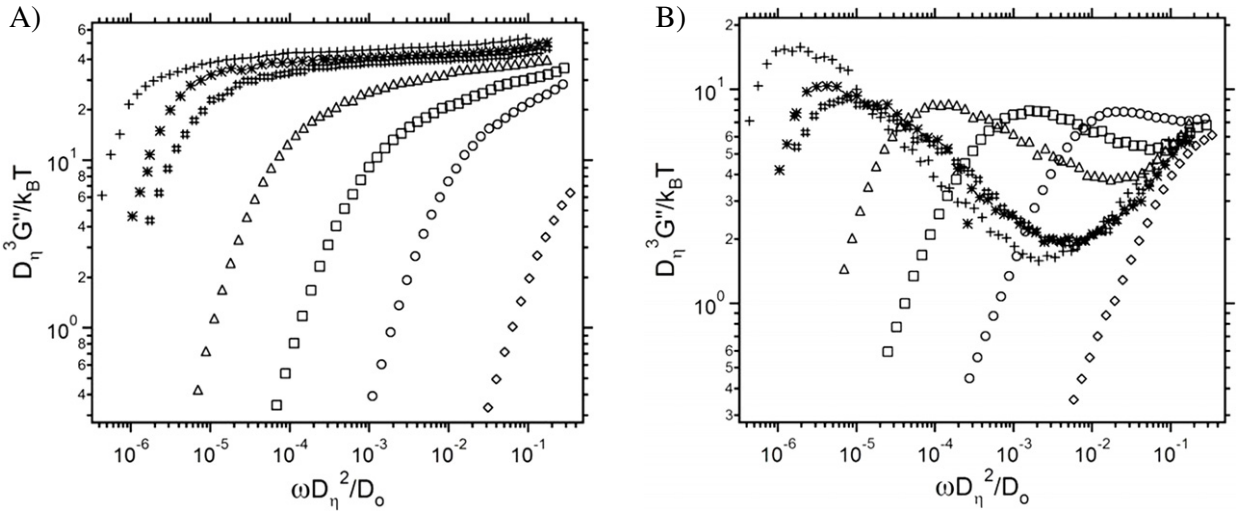

Figure 2. The linear dimensionless elastic, G', and viscous, G'', moduli for PEO400 is plotted versus dimensionless frequency. The effective volume fractions are $\phi_\eta = 0.535$ (◇), 0.569 (○), 0.575 (□), 0.581 (△), 0.587 (#), 0.592 (∗), and 0.598 (+).

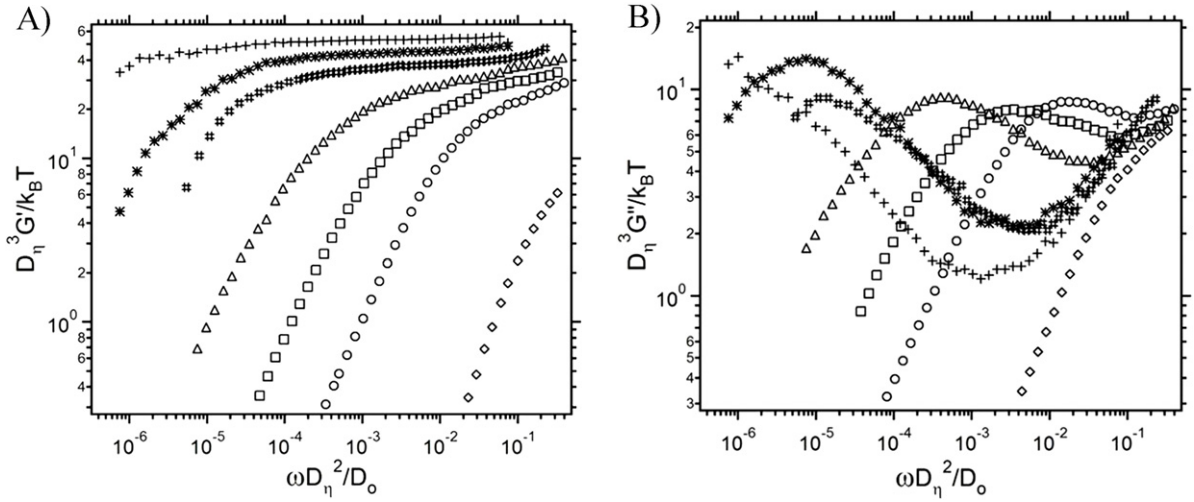

Figure 3. The linear dimensionless elastic, G', and viscous, G'', moduli for PEO1000 is plotted versus dimensionless frequency. The effective volume fractions in PEO1000 are $\phi_\eta = 0.515$ (◇), 0.568 (○), 0.573 (□), 0.578 (△), 0.583 (#), 0.588 (∗), and 0.594 (+).

particle volume fraction, $\phi_\eta = [1 + (2.9R_g/D_c)]\phi_c$ where D_c is the diameter of the core silica particles and $R_g/D_c = 0.019$ and 0.030 for PEO 400 and 1000, respectively. The ability of hard spheres to capture the viscosity of the PEO–silica nanocomposite suspensions motivates a comparison of these suspensions at higher volume fractions, where the nanocomposite suspensions become increasingly elastic, to other experimental hard sphere systems and to theoretical prediction of hard sphere glassy rheology.

Oscillatory rheology experiments were performed using a constant stress C-VOR Bohlin rheometer with cone and plate geometry. The cone diameter was 20 mm and the angle was 4°. Measurements were made at a sample temperature of 75 °C. Constant stress frequency sweeps measured the elastic, G', and viscous, G'', moduli in the linear viscoelastic regime. Strains were carefully monitored and kept near 10^{-3}. Single frequency stress sweeps measured the same moduli from strains of 10^{-3} to 1. Before measurement, the structure was broken down by preshearing the sample followed by a 5 min recovery time. The recovery was nearly instantaneous, but five minutes was given to ensure complete recovery.

3. Results and discussion

3.1. Linear rheology

In figures 2 and 3, we show frequency sweeps of the dimensionless elastic and viscous modulus in PEO400 and PEO1000 at effective volume fractions below and above 0.58. The moduli are non-dimensionalized by the effective particle hydrodynamic diameter, D_η, and by the thermal energy, k_BT, which is the product of Boltzmann's constant and the absolute temperature. The frequency is non-dimensionalized by D_η and the dilute self diffusion coefficient, $D_o = k_BT/3\pi\eta_p D_\eta$ where η_p is the polymer viscosity. As the volume fraction is raised,

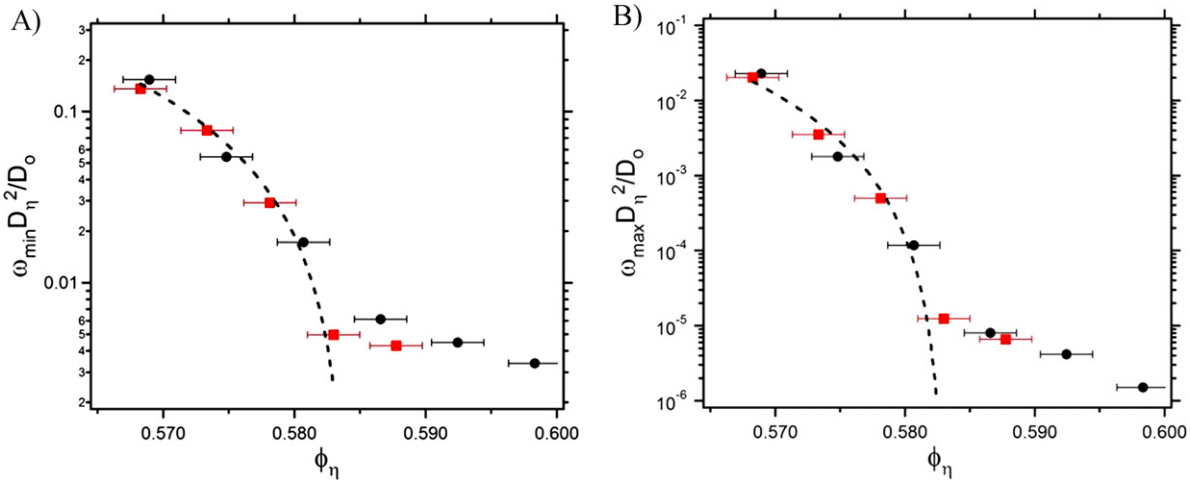

Figure 4. The (A) minimum and (B) maximum dimensionless frequency for PEO400 (●) and PEO1000 (■) plotted versus the effective particle volume fraction shows power law type divergence at low ϕ_η and decaying exponential behavior at high ϕ_η. The dashed line shows a power law fit at lower ϕ_η. The exponent for the minimum frequency is 1.5 ± 0.7 and for the maximum frequency is 3.0 ± 1.9 with a glass transition volume fraction of 0.583.

the elastic modulus plateaus at high frequency and increases in magnitude. The terminal flow regime shifts to lower frequency showing that longer times are needed for the dispersion to flow. Over the frequency range of the plateau in the elastic modulus, a minimum and a maximum develop in the viscous modulus with a depth and height that increase and shift to lower frequencies as the particle volume fraction is raised.

Using past extensions of MCT to the mechanical dynamics of glassy systems, we can understand the frequency behavior of the elastic and viscous moduli through the relaxation of particles trapped in nearest neighbor cages [9, 19, 20]. At high frequencies (short times), particles are unaware that they are caged and dynamics is dominated by the high frequency viscosity. A minimum develops in the viscous modulus as particle diffusion is limited by the cage. The minimum frequency in the viscous modulus is inversely proportional to the longest β relaxation time, τ_β, where particles are diffusing within a nearest neighbor cage. The frequency of the minimum in G'' corresponds to an inflection point in G'. As the frequency is reduced the viscous modulus passes through a minimum and increases to a maximum. In the region of increasing viscous modulus, there is a weak decrease in the elastic modulus after the point of inflection. Both phenomena reflect the dynamics of the α relaxation process when particles escape their cages thus dissipating energy stored by the cage. Near the end of the α process, the viscous modulus reaches a maximum and elastic modulus rolls off a plateau value marking the transition into the terminal regime. At very low frequencies (long times) particles are able to diffuse out of cages and the nanocomposite acts like a viscous fluid.

While predicted by MCT, for many years there was no direct experimental evidence showing how the relaxation of cages resulted in mechanical energy storage at short time and energy dissipation and flow at long time. A recent comparison of confocal microscopy measurements and computer simulations show that the frequency at the maximum in G'' and the loss of elasticity corresponds to the break up time, τ^*, of a percolated network of slowly relaxing glassy particle clusters [9]. Our experimental results showing the behavior of the linear moduli as a function of frequency agree with the simulation predictions in this study, thus connecting the glassy dynamics of silica dispersed in low molecular weight PEO to the cooperative rearrangement of percolating clusters.

Previous scattering studies have shown that the relaxation times characterizing the dynamics of colloidal suspensions approaching the glass transition display power law behavior as a function of the volume fraction [3, 4]. Here we test this scaling for the minimum, $\omega_{\min}$, and maximum, $\omega_{\max}$, frequencies. In figure 4, the dimensionless minimum and maximum frequency are plotted as a function of ϕ_η for PEO400 and PEO1000. The frequencies of both molecular weights collapse reasonably well when rescaled by D_η and D_o. In addition, figure 5 shows a collapse of the moduli at these two characteristic frequencies indicating a hard sphere like scaling for changes in continuous phase viscosity and effective particle size. For $\phi_\eta \leqslant 0.584$, $\omega_{\min}$ and $\omega_{\max}$ decrease in a critical manner that is well described by $\omega \sim (1 - \phi/\phi_g)^\lambda$ with $\lambda = 1.5 \pm 0.7$ and $\phi_g = 0.583$ for $\omega_{\min}$ and $\lambda = 3.0 \pm 1.9$ and $\phi_g = 0.584$ for $\omega_{\max}$. For hard sphere glasses, MCT predicts power exponents of 1.66 and 2.58 for the β and α relaxation processes respectively and $\phi_g = 0.525$ [10–12]. The predicted exponents of MCT theory were shown to agree reasonably well with a dynamic light scattering (DLS) study of particle diffusivities in hard sphere like polymethylmethacrylate particle suspensions with a $\phi_g = 0.57$ [4]. The exponents found for $\omega_{\min}$ and $\omega_{\max}$ are comparable within experimental uncertainty with the MCT exponents.

In the PEO–silica nanocomposite suspensions at volume fractions greater than ϕ_g, we still see a $\omega_{\min}$ and a $\omega_{\max}$ giving the appearance that relaxations continue contrary to what is predicted for an ideal glass transition albeit the behavior as a function of volume fraction has changed. Above $\phi_g = 0.583$, the volume fraction dependence of $\omega_{\min}$ and $\omega_{\max}$ can be described by a decaying exponential. Interestingly, the DLS

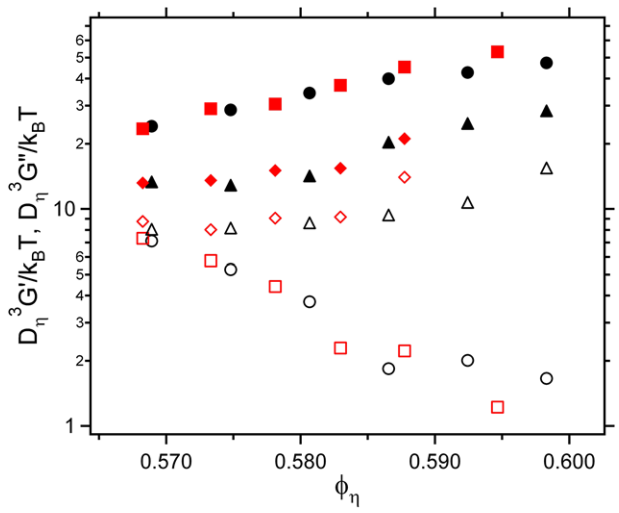

Figure 5. The dimensionless elastic modulus (solid symbols) and viscous modulus (open symbols) at the minimum (circles, squares) and maximum (triangles, diamonds) dimensionless frequencies are plotted versus the effective particle volume fraction in PEO400 (circles, triangles) and PEO1000 (squares, diamonds).

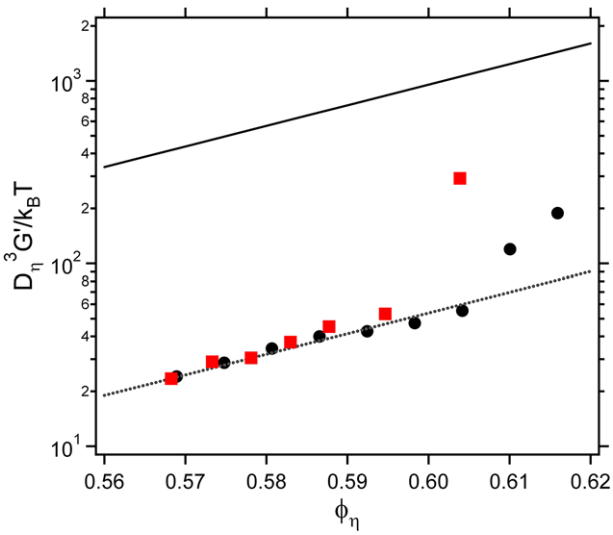

Figure 6. The dimensionless linear elastic modulus at the point of inflection within the frequency plateau is plotted versus the effective particle volume fraction in PEO400 (●) and PEO1000 (■). The solid line is the prediction of no adjustable parameter theory and the dotted line is the rescaled theory with the same functional dependence on volume fraction [15].

study also shows the beginnings of a decay in the intermediate scattering function (ISF) at volume fractions in excess of ϕ_g suggesting the appearance of continued terminal relaxation behavior above ϕ_g.

The change in the functional form of the minimum and maximum frequency above ϕ_g suggests a new mechanism for stress relaxation within the glass. MCT predicts an idealized glass transition where particles become permanently caged and long time self diffusivity goes to zero. As a result, within MCT, the glass is characterized by structural arrest. Our results are in agreement with the predictions of MCT for $\phi/\phi_g < 1$, but demonstrate continued relaxation when $\phi/\phi_g > 1$. While the mechanism is not entirely understood as fast moving particles are isolated, long range particle diffusion is observed above the glass transition volume fraction [6, 9]. The presence of single fast moving particles above the glass transition may support the existence of activated hopping processes capable of relieving internal stress in the glass. However, the authors of the DLS study attribute the decay above ϕ_g to non-ergodic time evolution since the ISF was found to change depending on the waiting time between measurements and did not stabilize to a time insensitive function up to waiting times of 10^7 s [4].

Schweizer and coworkers have constructed a theoretical framework that includes the microstructure cage correlations of MCT at the single particle level with a free energy landscape approach that controls particle dynamics [14, 15]. The theory does not include coupling of dynamic density fluctuations and is therefore not influenced by an ideal glass transition. Kobelev and Schweizer [15] predict the zero stress dimensionless elastic modulus to have an exponential dependence on the volume fraction:

$$\frac{D^3 G'}{k_B T} = (1.6 \times 10^{-4}) e^{26\phi}. \tag{3.1}$$

This equation is calculated from the theoretical model using Percus–Yevick structural input of hard sphere equilibrium microstructures.

In figure 6, we plot the linear elastic modulus at the point of inflection of G' which corresponds to the minimum frequency in the viscous modulus. The elastic modulus prediction of Kobelev and Schweizer is also shown in figure 6. Three additional data points extend the results up to $\phi_\eta = 0.616$ in PEO400 and one additional data point extend the results in PEO1000 up to $\phi_\eta = 0.604$. The last two data points in PEO400 show a break in the data such that G' appears to be a stronger function of ϕ_η. A similar trend is seen in PEO1000 for the last data point. The transition is attributed to the onset of polymer confinement effects.

Studies of the mechanical properties of polymer confined between surfaces show that as surface separations approach the size of the polymer molecule, namely R_g, the viscosity of the polymer between the surfaces increases above the bulk value. When surface separations are greater than the confinement condition, the viscosity of the film is comparable to the bulk viscosity with a no slip boundary condition located above the surface at a distance that scales on R_g [21–24]. Confinement effects in the PEO-silica nanocomposite set in when the particle surface separation, $a_{cc} = (D_c/R_g)[(\phi_m/\phi_c)^{1/3} - 1]$ is reduced from $3.7R_g$ at $\phi_\eta = 0.604$ to $3.5R_g$ at $\phi_\eta = 0.610$ in PEO400. Here ϕ_m is the maximum random packing fraction of 0.63. This result suggests that for $\phi_\eta \leqslant 0.604$, the unentangled PEO400 nanocomposite melt can be mechanically treated as particles with a size D_η dispersed in a polymer continuum. When $\phi_\eta > 0.604$, the confined polymer enhances the nanocomposite melt viscosity. In the PEO1000 nanocomposite, confinement sets in when $\phi_\eta > 0.594$ where the surface separation in PEO1000 is $3.6R_g$. For $\phi_\eta \leqslant 0.604$ in PEO400 and $\phi_\eta \leqslant 0.594$ in PEO1000, we expect the hard sphere treatment of the nanocomposite to be applicable.

A direct comparison of the theory and the data shows that the theory over predicts the elastic modulus of the suspensions

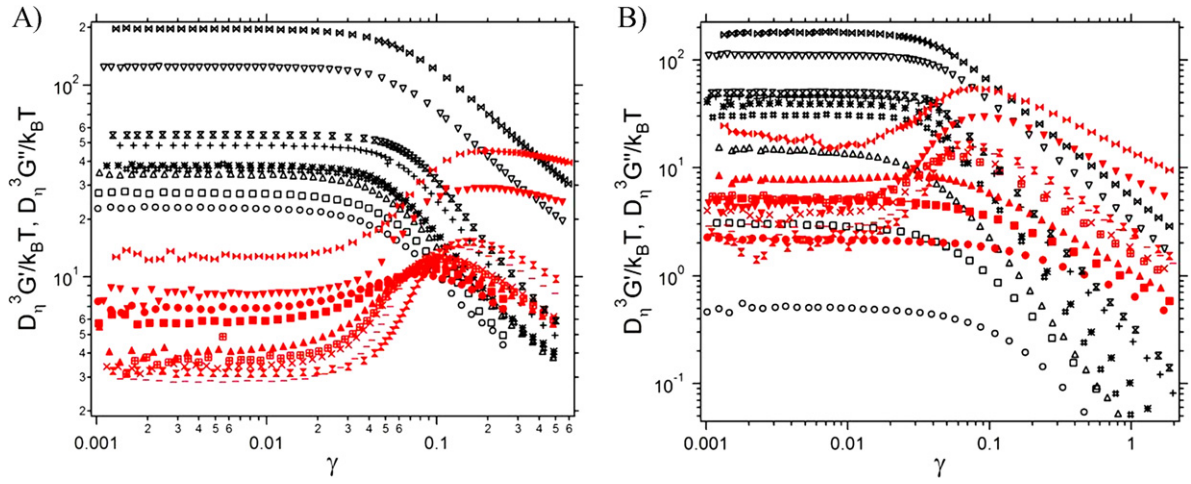

Figure 7. The non-linear elastic and viscous moduli for PEO400 at (A) 10 Hz and (B) 0.1 Hz versus strain. The effective volume fractions are $\phi_\eta = 0.569$ (○, ●), 0.575 (□, ■), 0.581 (△, ▲), 0.587 (#, ⊞), 0.592 (∗, ×), 0.598 (+, −), 0.604 (⧗, ⧖), 0.610 (▽, ▼), and 0.615 (⋈, ⧓).

by a factor of ∼18. However, the functional dependence of G' on the volume fraction is well captured by the theory when the prediction is scaled down. When fitting the data to an exponential of the form $Ae^{b\phi}$, b is 24 ± 2 showing close agreement with the predictions. The data can also be well fit by a power law of the form $A\phi^n$ where n is 14 ± 1. Power law fitting of the theoretical predictions gives an exponent of 14 again showing agreement between our measurements and the predictions. Over prediction by the theory is common when compared to other experimental hard sphere systems and can be attributed to using the Percus–Yevick structure factor as the structural input in the theory and/or to particle softness [15, 25].

3.2. Non-linear rheology

Non-linear elastic and viscous moduli of dense nanocomposite suspensions from controlled stress sweeps at dimensional (dimensionless) measurement frequencies, ω_{meas}, of 10 Hz (4.1×10^{-2}) and 0.1 Hz (4.1×10^{-4}) as a function of strain are shown for different volume fractions in figure 7. At 10 Hz, in the large strain limit when $\phi_\eta \leqslant 0.604$, the moduli decrease with power law slopes of $G' \propto \gamma^{-1}$ and $G'' \propto \gamma^{-0.5}$. A perturbative yield point, defined as the strain where the elastic modulus reaches 0.9 of its low strain plateau value, is reached at a strain of ∼0.03 for all volume fractions. The viscous modulus develops a peak as the volume fraction is raised. This maximum in loss behavior occurs initially at a strain of 0.07 at $\phi_\eta = 0.569$ and shifts over to 0.11 at $\phi_\eta = 0.604$. At a frequency of 0.1 Hz in figure 7(B), the perturbative yield strain still occurs at a value of 0.03, but the peak in G'' is only observed for $\phi_\eta \geqslant 0.581$. The peak is first observed at a strain of 0.035 and shifts to a value of 0.07 for $\phi_\eta = 0.604$. In the large strain limit, the terminal elastic modulus decreases as $G' \propto \gamma^{-1.7}$. When there is no peak in G'', the terminal power law is $G'' \propto \gamma^{-0.7}$, and when there is a peak in G'', the terminal power law is $G'' \propto \gamma^{-0.8}$. If the strain at the peak in G'' is compared at the same ϕ_η but at different measurement frequency, the peak occurs at a lower strain at 0.1 Hz than at 10 Hz demonstrating that less deformation is needed to break up the structure at lower frequencies.

When $\phi_\eta > 0.604$ in PEO400, the yielding of the suspensions is influenced by confinement of the polymer. This is seen in two areas. First, at low strain when $\phi_\eta > 0.604$, small increases in ϕ_η result in a jump in the rate increase in G' as volume fraction is increased. Secondly, at high strain, the terminal decline in G' and G'' are characterized by weaker power law decays. In the large strain limit, for $\phi_\eta > 0.604$, $G' \propto \gamma^{-0.8}$ and $G'' \propto \gamma^{-0.2}$ at 10 Hz and $G' \propto \gamma^{-1.1}$ and $G'' \propto \gamma^{-0.6}$ at 0.1 Hz. The weaker decay suggests that the applied strains are not sufficient to drive the suspension into terminal behavior. We associate this with the confined polymer resisting complete break up of cage microstructure. Measurements at higher strain were frustrated by slip between the nanocomposite melt and the rheometer tools.

In section 3.1, it was noted that ω_{max} is related to the break up time of a percolated network of slowly relaxing glassy clusters such that the suspension lies in the terminal, liquid-like region when $\omega < \omega_{max}$. We associate the onset of the maximum in G'' with increasing strain with the state of the suspension in the zero strain limit. Shown in figure 8 are dimensionless elastic and viscous moduli for a suspension with $\phi_\eta = 0.575$. The frequency of the applied stress sweep, ω_{meas}, is shown under three conditions: $\omega_{meas}/\omega_{max} > 1$, $\omega_{meas}/\omega_{max} \sim 1$, and $\omega_{meas}/\omega_{max} < 1$ where at this volume fraction $\omega_{max} = 0.46$ Hz. These stress sweeps clearly show the onset of the maximum in G'' growing in when $\omega_{meas}/\omega_{max} \sim 1$ with the strain at the maximum growing with strain frequency. Notice that the low strain viscous modulus passes through a maximum when $\omega_{meas}/\omega_{max} \sim 1$. This result is simply a restatement of the data in figures 2 and 3 where in the low strain limit G'' passes through the viscous maximum at ω_{max}. These experiments were chosen to illustrate the disappearance of the maximum in G'' at larger strains when ω_{meas} becomes less than ω_{max} and is typical of other systems investigated. For $\omega_{meas}/\omega_{max} < 1$, the clusters have the opportunity to relax. For $\omega_{meas}/\omega_{max} > 1$, the strain frequency is sufficiently fast that thermal motion is insufficient to disrupt the cages and

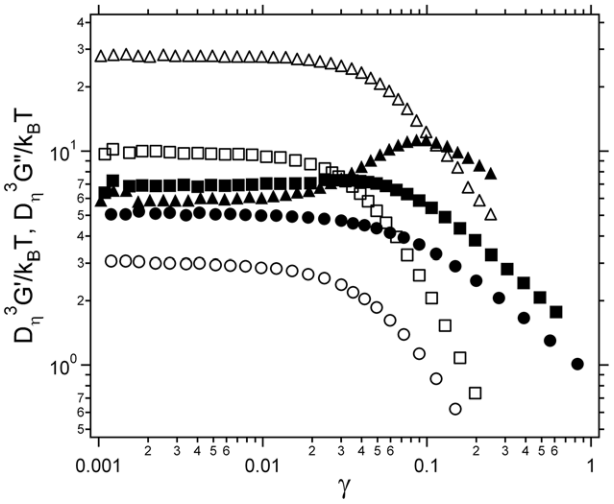

Figure 8. The non-linear elastic and viscous moduli for PEO400 at $\phi_\eta = 0.575$ at measurement frequencies, ω_{meas}, of 0.1 Hz (○, ●), 0.5 Hz (□, ■), and 10 Hz (△, ▲).

there is increased dissipation at a strain associated with cage degradation.

Due to the similarity of the mechanical behavior of the nanocomposite suspensions studied here to that of hard spheres suspended in a low molecular weight continuous phase, we are interested in how well the strain softening and yield of the glassy nanocomposite suspensions compare to theoretical predictions of hard sphere glasses. For such systems, Kobelev and Schweizer extend the naïve MCT free energy landscape model to predict an absolute yield point where, in the absence of hoping motions, the energy barrier to hopping drops to zero and a perturbative yield point where the elastic modulus drops to 0.9 of the zero stress limit. The absolute yield stress is predicted to occur at strains in excess of 0.1 and is found to lie near strains where $G' = G'' = G_x$ in the stress sweeps. For purposes of comparison with the scaling predicted by Kobelev and Schweizer we choose G_x as a surrogate for the position of the absolute yield point.

In figure 9(A), the stress, σ_x, at G_x, the dimensionless value of G_x, and the strain, γ_x, at G_x are shown as a function of ϕ_η. At 10 Hz, $\omega_{meas}/\omega_{max} > 1$ for all ϕ_η shown. As a result these samples are always glassy in the low strain limit. The dependence of σ_x, G_x, and γ_x on ϕ_η changes near $\omega_{meas}/\omega_{max} = 1$ as seen near $\phi_\eta = 0.58$ and $\phi_\eta = 0.585$ for 1 and 0.1 Hz, respectively. At 0.1 Hz for $\phi_\eta \leqslant 0.575$, G'' is larger than G' at low strain (figure 7(A)) because ω_{meas} is less than the frequency where the linear moduli cross (figure 4). These nanocomposites behave as viscous liquids at a frequency of 0.1 Hz. At 1 Hz, ω_{meas} is always greater than the frequency where the limiting low strain moduli cross but the values of σ_x, G_x, and γ_x remain sensitive to proximity of ω_{meas} to ω_{max}. Since ω_{max} decreases rapidly as ϕ_η increases, for all ϕ_η where $\omega_{meas} > \omega_{max}$, the glassy yielding behavior of the nanocomposite melts and the volume fraction dependencies of σ_x, G_x, and γ_x are similar to the behavior at 10 Hz.

We compare the predictions of Kobelev and Schweizer with the values of G_x measured at 10 Hz as $\omega_{meas}/\omega_{max} > 1$ for all ϕ_η reported in figure 9. The prediction of the stress, elastic modulus, and strain at the absolute yield point are drawn as solid lines. Kobelev and Schweizer indicate that the predicted dimensionless stress, $D^3\sigma_{abs}/k_BT$, is equally well fit by an exponential and a power law of the forms $Ae^{b\phi}$ and $B\phi^n$, respectively, with $A = 6.16 \times 10^{-4}$ and $b = 19.2$ and $B = 1.72 \times 10^4$ and $n = 11$. The experimental results are lower than the prediction. When rescaling the theory to the initial magnitude of the stress at $\phi_\eta = 0.568$, we find that the exponential prediction of the absolute yield stress on volume fraction fits the data reasonably well up to $\phi_\eta = 0.592$ but falls off of the data at higher ϕ_η. A power law fit of the data up to $\phi_\eta = 0.604$ prior to confinement fit the data reasonably well with $B = 2.1 \times 10^4$ and $n = 17 \pm 1$ shown by the dashed in figure 9(A). An exponential also provides a reasonable fit when $b = 28 \pm 1$ and $A = 1.4 \times 10^{-7}$.

A similar analysis is applied to G_x shown in figure 9(B). The predicted absolute yield elastic modulus of Kobelev and Schweizer is well fit by a power law with coefficient and exponent of $B = 1.89 \times 10^5$ and $n = 12.9$. The rescaled theory shown by the dotted line does not fit the data. We find a reasonable fit to a power law prior to confinement with $B = 330$ and $n = 6.2 \pm 0.5$.

The crossover strain, γ_x, in figure 9(C) increases at all three frequencies with ϕ_η prior to confinement. The opposite trend is predicted for hard sphere glasses by Kobelev and Schweizer. Once the polymer is confined, γ_x sharply increases followed by a decrease at 0.1 and 1 Hz, while at 10 Hz there is still an increase. Thus, while the hard sphere model captures much of the linear mechanical behavior of this unentangled polymer nanocomposite melt, the presence of the polymer or our association of σ_x with the absolute yield stress in the theory appear to compromise predictions of the absolute yield strain.

In figure 10, we present results for the stress, moduli, and strain at the perturbative yield point. When the polymer is unconfined, the proximity of ω_{meas} to ω_{max} at 0.1 and 1 Hz influences measurement of the perturbative yield values. The theory is only compared to σ_y at 10 Hz since the yielding behavior at this frequency shows the stress accelerated break up of glassy particle domains for all volume fractions. Once the polymer is confined, the perturbative yield stress, moduli, and strain change as a function of ϕ_η.

Kobelev and Schweizer show that the perturbative yield stress, σ_y, predicted by the theory is well fit by a power law with $B = 880$ and $n = 8.6$. When the theory is rescaled to the magnitude of σ_y at $\phi_\eta = 0.568$ shown by the dotted line in figure 10(A), the predicted power law does not capture the trend of the data. We find a much stronger power law dependence of $n = 23 \pm 2$ with $B = 2.5 \times 10^5$ when fitting σ_y up to $\phi_\eta = 0.604$.

The rescaled prediction of the perturbative yield elastic modulus agrees well with the data. The prediction of G'_y is of the same form as the prediction for the zero stress elastic modulus but the coefficient is reduced by 10%. After polymer confinement, σ_y and G'_y jump in value and become a stronger function of ϕ_η. Prior to polymer confinement, G''_y is a decreasing function of ϕ_η. As the polymer is confined, G''_y also becomes an increasing function of ϕ_η.

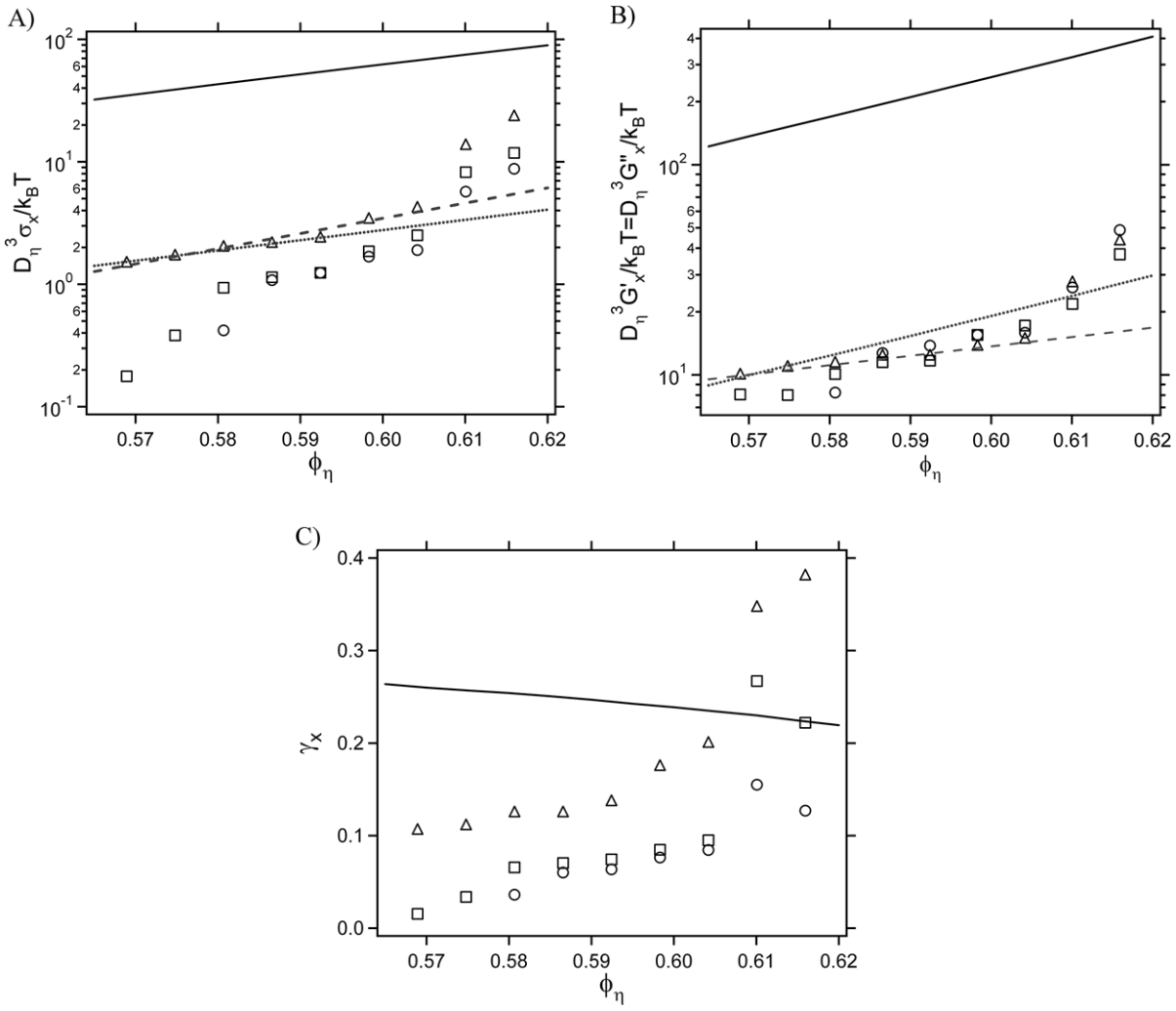

Figure 9. (A) The stress, σ_x, at the point where the elastic and viscous moduli are equal versus the effective volume fraction at frequencies of 0.1 Hz (circles), 1 Hz (squares), and 10 Hz (triangles). The solid line is the predicted absolute yield values of Kobelev and Schweizer and the dotted line is the rescaled predictions down to the initial magnitude at $\phi_\eta = 0.568$ [15]. The dashed line is power law fits of σ_x at 10 Hz for $\phi_\eta \leqslant 0.604$. (B) The moduli, G_x, at the point where the elastic and viscous moduli are equal versus the effective volume fraction at frequencies of 0.1 Hz (circles), 1 Hz (squares), and 10 Hz (triangles). The solid line is the predicted absolute yield values of Kobelev and Schweizer and the dotted line is the rescaled predictions down to the initial magnitude at $\phi_\eta = 0.568$ [15]. The dashed line is power law fits of G_x at 10 Hz for $\phi_\eta \leqslant 0.604$. (C) The strain, γ_x, at the point where the elastic and viscous moduli are equal versus the effective volume fraction at frequencies of 0.1 Hz (circles), 1 Hz (squares), and 10 Hz (triangles). The solid line is the predicted absolute yield values of Kobelev and Schweizer [15].

The perturbative yield strain, γ_y is a decreasing function of ϕ_η when $\omega_{\text{meas}} < \omega_{\max}$. Once $\omega_{\text{meas}} > \omega_{\max}$ (prior to polymer confinement), γ_y increases with ϕ_η at all three frequencies. The theory of Kobelev and Schweizer predicts that γ_y is a decreasing function of ϕ_η when suspensions are in the glassy state contrary to what is seen here. Once the polymer is confined, γ_y shows a change at the point of confinement such that the strain decreases.

Differences between the experimental and predicted yield parameters may be a result of the theory being developed for hard spheres with no regard for the dispersing phase being a polymer melt. The connectivity of polymer segments may be influencing the yielding mechanism of the nanocomposites. In addition, the non-linear behavior of the polymer nanocomposites demonstrates the effect of strain frequency on the strain dependence of the moduli at different frequencies. This type of frequency dependence is currently not in the model.

4. Conclusion

In this paper, the mechanical properties of suspensions of nanoparticles dispersed in a low molecular weight polymer melt are characterized. The particles have a similar refractive index to the polymer which minimizes particle van der Waals forces, and viscosity measurements at dilute to concentrated volume fractions show that particle interactions are hard sphere like in the polymer melt due to the formation of an adsorbed polymer layer on the particle surface. This comparison suggests that the growth of elasticity in the nanocomposite at

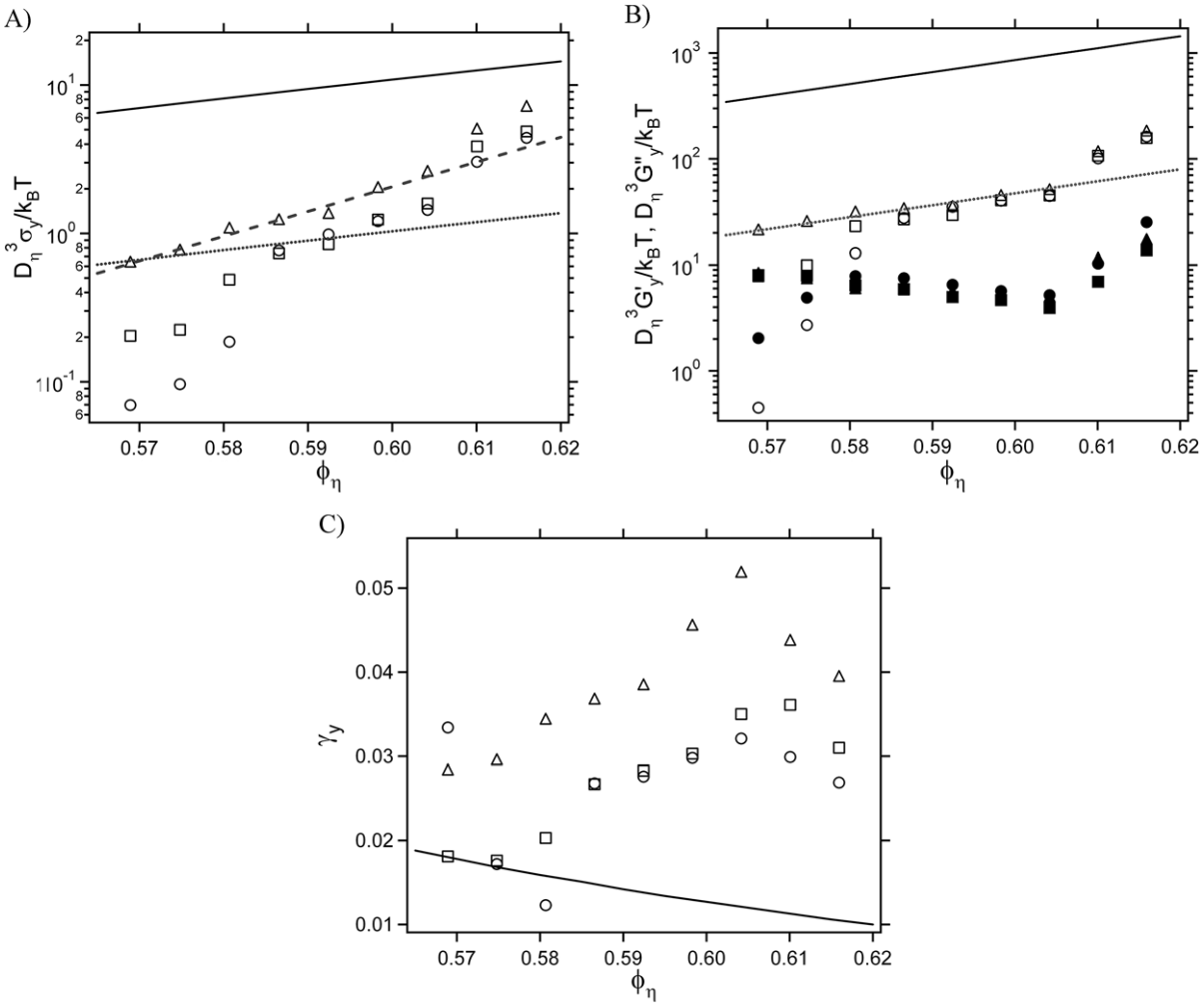

Figure 10. (A) The perturbative yield stress, σ_y, versus the effective volume fraction at frequencies of 0.1 Hz (circles), 1 Hz (squares), and 10 Hz (triangles). The solid line represents the predictions of Kobelev and Schweizer [15]. The dotted line is the rescaled theory down to the initial magnitude of the perturbative yield at 10 Hz. The dashed line is a power law fit of σ_y at 10 Hz for $\phi_\eta \leqslant 0.604$. (B) The elastic modulus, G'_y, (open symbols) and viscous modulus, G''_y, (closed symbols) at the perturbative yield versus the effective volume fraction at frequencies of 0.1 Hz (circles), 1 Hz (squares), and 10 Hz (triangles). The solid line represents the predictions of Kobelev and Schweizer [15]. The dotted line is the rescaled theory down to the initial magnitude of the perturbative yield at 10 Hz. (C) The perturbative yield strain versus the effective volume fraction at frequencies of 0.1 Hz (circles), 1 Hz (squares), and 10 Hz (triangles). The solid line represents the predictions of Kobelev and Schweizer [15].

high volume fractions signals the onset of a colloidal glass transition.

As the effective particle volume fraction approaches 0.58, dynamic mechanical measurement of the linear elastic and viscous moduli show the emergence of a plateau elastic modulus at high frequency and characteristic frequencies in the viscous modulus which define two relaxation processes in the nanocomposite melt. At volume fractions less than the glass transition value of 0.583, the volume fraction dependencies of both characteristic frequencies and the magnitude of the plateau elastic modulus are captured reasonably well by theoretical predictions of hard sphere glasses. This leads to the conclusion that the origin of elasticity in the concentrated unentangled nanocomposite melt is due to the formation of a colloidal glass. These materials do not show an idealized glass transition since an exponentially decreasing terminal relaxation frequency is observed above the glass transition volume fraction.

Yielding of the concentrated nanocomposite melt was studied via stress controlled oscillatory shear sweeps. We show that the non-linear yielding of the suspensions is influenced by the oscillatory frequency of the stress sweep and by the proximity of the oscillatory frequency to the frequency at the maximum in the linear viscous modulus indicating the terminal relaxation timescale of the nanocomposite. At high oscillatory frequency, the suspensions show glassy behavior at all volume fractions studied here. The non-linear yielding of the suspension is described by the breakup of percolated glassy domains. At lower frequencies, the non-linear rheology of the suspension is influenced by the timescale for thermal particle motion to relax glassy domains in the suspension.

Little agreement is seen in a comparison between the non-linear elastic modulus, yield stress, and yield strain of the concentrated nanocomposites and the non-linear yielding theory of Schweizer and co-workers. Explanations for the differences may lie in the cooperative nature of particle

dynamics that is known to function in the relaxation of glasses and is not included in the model and in activated hopping process which are later incorporations into the model. The differences between the model and the nanocomposites may also result from contributions of the polymeric nature of the continuous phase such that connectivity of polymer segments may influence the yielding mechanism of the nanocomposite melt.

Acknowledgments

The authors would like to thank Ken Schweizer for helpful discussions regarding the dynamics of glassy suspensions. This work was supported by the Nanoscale Science and Engineering Initiative of the National Science Foundation under NSF Award Number DMR-0642573.

References

[1] Angell C A 1995 Formation of glasses from liquids and biopolymers *Science* **267** 1924–35
[2] van Blaaderen A and Wiltzius P 1995 Real-space structure of colloidal hard-sphere glasses *Science* **270** 1177–9
[3] van Megen W and Underwood S M 1994 Glass transition in colloidal hard spheres: measurement and mode-coupling-theory analysis of the coherent intermediate scattering function *Phys. Rev.* E **49** 4206
[4] van Megen W *et al* 1998 Measurement of the self-intermediate scattering function of suspensions of hard spherical particles near the glass transition *Phys. Rev.* E **58** 6073–85
[5] Kegel W K and van Blaaderen A 2000 Direct observation of dynamical heterogeneities in colloidal hard-sphere suspensions *Science* **287** 290–3
[6] Weeks E R *et al* 2000 Three-dimensional direct imaging of structural relaxation near the colloidal glass transition *Science* **287** 627–31
[7] Debenedetti P G 1996 *Metastable Liquids* (Princeton, NJ: Princeton University Press)
[8] Weeks E R and Weitz D A 2002 Properties of cage rearrangements observed near the colloidal glass transition *Phys. Rev. Lett.* **89** 095704
[9] Conrad J C *et al* 2006 Contribution of slow clusters to the bulk elasticity near the colloidal glass transition *Phys. Rev. Lett.* **97** 265701
[10] Barrat J L, Gotze W and Latz A 1989 The liquid–glass transition of the hard-sphere system *J. Phys.: Condens. Matter* **1** 7163–70
[11] Bengtzelius U, Gotze W and Sjolander A 1984 Dynamics of supercooled liquids and the glass transition *J. Phys. C: Solid State Phys.* **17** 5915–34
[12] Fuchs M, Hofacker I and Latz A 1992 Primary relaxation in a hard-sphere system *Phys. Rev.* A **45** 898
[13] Saltzman E J and Schweizer K S 2003 Transport coefficients in glassy colloidal fluids *J. Chem. Phys.* **119** 1197–203
[14] Schweizer K S and Saltzman E J 2003 Entropic barriers, activated hopping, and the glass transition in colloidal suspensions *J. Chem. Phys.* **119** 1181–96
[15] Kobelev V and Schweizer K S 2005 Strain softening, yielding, and shear thinning in glassy colloidal suspensions *Phys. Rev.* E **71** 021401
[16] Saltzman E J and Schweizer K S 2006 Activated hopping and dynamical fluctuation effects in hard sphere suspensions and fluids *J. Chem. Phys.* **125** 044509
[17] Schweizer K S and Saltzman E J 2004 Activated hopping, barrier fluctuations, and heterogeneity in glassy suspensions and liquids *J. Phys. Chem.* B **108** 19729–41
[18] Anderson B J and Zukoski C F 2008 Rheology and microstructure of an unentangled polymer nanocomposite melt *Macromolecules* **41** 9326–34
[19] Banchio A J, Nagele G and Bergenholtz J 1999 Viscoelasticity and generalized Stokes–Einstein relations of colloidal dispersions *J. Chem. Phys.* **111** 8721–40
[20] Mason T G and Weitz D A 1995 Linear viscoelasticity of colloidal hard sphere suspensions near the glass transition *Phys. Rev. Lett.* **75** 2770
[21] Granick S and Hu H-W 1994 Nanorheology of confined polymer melts. 1. Linear shear response at strongly adsorbing surfaces *Langmuir* **10** 3857–66
[22] Granick S, Hu H-W and Carson G A 1994 Nanorheology of confined polymer melts. 2. Nonlinear shear response at strongly adsorbing surfaces *Langmuir* **10** 3867–73
[23] Israelachvili J N and Kott S J 1988 Liquid structuring at solid interfaces as probed by direct force measurements: the transition from simple to complex liquids and polymer fluids *J. Chem. Phys.* **88** 7162–6
[24] Luengo G *et al* 1997 Thin film rheology and tribology of confined polymer melts: contrasts with bulk properties *Macromolecules* **30** 2482–94
[25] Rao R B *et al* 2006 Nonlinear elasticity and yielding of nanoparticle glasses *Langmuir* **22** 2441–3
[26] Cheng Z *et al* 2002 Nature of the divergence in low shear viscosity of colloidal hard-sphere dispersions *Phys. Rev.* E **65** 041405